Pergamon

Int. J. Heat Mass Transfer. Vol. 38, No. 15, pp. 2707–2714, 1995

0017–9310/95 $9.50+0.00

0017–9310(95)00077–1

Effect of internal radiation within crystal and melt on Czochralski crystal growth of oxide

TAKAO TSUKADA, KATSUYUKI KAKINOKI and MITSUNORI HOZAWA
Institute for Chemical Reaction Science, Tohoku University, Sendai 980, Japan

and

NOBUYUKI IMAISHI

Institute of Advanced Material Study, Kyushu University, Kasuga 816, Japan

(*Received* 2 *December* 1994 *and in revised form* 23 *February* 1995)

Abstract—For the crystal growth of an oxide, a global analysis of heat transfer in the inductively heated Czochralski furnace was carried out, taking the radiative heat transfer within the crystal and the melt into account. As a result, the flow and temperature fields are strongly affected by the variation in optical properties of the crystal and the melt, and the melt–crystal interface shape becomes more convex to the melt as the optical absorption coefficients of both the crystal and the melt decrease.

1. INTRODUCTION

Oxide single crystals such as yttrium aluminum garnet (YAG), gadolinium gallium garnet (GGG) and lithium niobate (LN) are utilized as solid-state laser hosts and materials for acoust-opt-electronics devices, and are commonly grown by the Czochralski (CZ) method. For the production of a perfect single crystal by this method, it is important to acquire the correct information about the heat transfer mechanism and to control the heat transfer in the CZ furnace, because the quality of the crystal is closely related to its thermal history and the transport phenomena in the furnace.

One of the methods of predicting the phenomena in the CZ furnace for oxide crystal growth is numerical simulation. Kobayashi [1, 2] and Langlois [3] have modeled the CZ oxide crystal growth system using the so-called 'bulk flow' model, which considered only the heat transfer and fluid mechanics in the fixed-geometry melt. More rigorous models [4–9] have now been developed which account for both the melt–crystal and melt–gas interface shapes in addition to heat transfer in the melt and the crystal and the melt convection, but they employ the assumption that temperatures at the crucible or the heater and at the ambient wall are all given. Recently, the global heat transfer analysis was developed for the CZ crystal growth of an oxide [10, 11], where one could predict the temperature and flow fields in the furnace and all interface shapes under the given furnace geometry and processing conditions.

Oxide crystals are not opaque to infrared radiation. This strongly influences heat transfer and the melt–crystal interface shape during the CZ crystal growth. For instance, the internal radiation through the crystal makes the interface deeply convex toward the melt. Cockayne *et al.* [12] and Kvapil *et al.* [13] studied the effect of optically active dopants on the interface shape in the CZ oxide growth system, and revealed that the optical absorption characteristics of the crystal affects the interface deflection. However, most of the mathematical models in the previous theoretical studies have not taken this effect into account.

Recently, Xiao and Derby [14, 15] modeled the internal radiation within the crystal during the CZ crystal growth of GGG and YAG, and numerically demonstrated the deeply convex interfaces. However, their model approximated the internal radiation through the crystal by considering the crystal to be totally transparent and bounded by vanishingly thin opaque surfaces, and thus could not account for the effect of the optical properties, e.g. absorption coefficient of the semitransparent crystal, which is encountered with the addition of various amounts of dopants in Cockayne's experimental work. The more rigorous approach for modeling the internal radiation is necessary in the CZ system, as attempted in the Bridgeman system by Brandon and Derby [16, 17] and Matsushima and Viskanta [18].

The aim of this work is to develop a global analysis of heat transfer in the inductively heated CZ furnace, in which the internal radiative heat transfer within the

NOMENCLATURE

A'	area of surface element [m^2]
A	$=A'/r_c'^2$
a'	optical absorption coefficient [m^{-1}]
a	optical thickness ($=a'r_c'$)
C_p	heat capacity [J kg^{-1} K^{-1}]
F_{jk}	view factor
G_{jk}	the fraction of the outgoing radiative flux from surface A_j that reaches A_k
Gr	Grashof number ($=r_c'^3\beta T_m' g/\nu_l^2$)
g	gravitational acceleration [m s^{-2}]
ΔH_s	latent heat of solidification [J kg^{-1}]
i'	radiative intensity [W m^{-2} sr^{-1}]
J'	irradiance [W m^{-2}]
J	$=J'/4\sigma T_m'^4$
k	thermal conductivity [W m^{-1} K^{-1}]
N_R	radiation–condution interaction parameter ($=4\sigma T_m'^3 r_c'/k_l$)
n	refractive index
n	normal vector at the boundary surface
Pe	Peclet number ($=\rho_{0s}C_{ps}V_s'r_c'/k_l$)
Pr	Prandtl number ($=\mu_l C_{pl}/k_l$)
$q_i^{in'}$	incoming radiative flux from the inside of the boundary surface [W m^{-2}]
$q_i^{out'}$	incoming radiative flux from the surroundings to the boundary surface [W m^{-2}]
q_i^{in}, q_i^{out}	$=q_i^{in'}$, $q_i^{out'}/\sigma T_m'^4$
r'	radial distance in cylindrical coordinates [m]
r_c'	crucible radius [m]
r	$=r'/r_c'$
St	Stefan number ($=\Delta H_s/C_{ps}T_m'$)
T'	temperature [K]
T_m'	melting point temperature [K]
T	$=T'/T_m'$
u'	radial component of velocity vectors [m s^{-1}]
V_s'	crystal pulling rate [m s^{-1}]
w'	axial component of velocity vectors [m s^{-2}]
u, w	$=u'r_c'/\nu_l$, $w'r_c'/\nu_l$
z'	axial distance in cylindrical coordinates [m]
z	$=z'/r_c'$.

Greek symbols

β	thermal expansion coefficient [K^{-1}]
ε	emissivity
μ	viscosity [Pa s]
ν	kinematic viscosity [m^2 s^{-1}]
κ	$=k/k_l$
ρ_0	density [kg m^{-3}]
ρ	reflectivity
σ	Stefan–Boltzman constant [W m^{-2} K^{-4}]
τ	transmissivity
ω	solid angle [sr].

Subscripts

c	crucible
k	materials other than crystal, melt and crucible
l	melt
s	crystal.

crystal and the melt can be accounted for, and to reveal the effect of optical properties on the velocity and temperature distributions in the furnace and on the melt–crystal interface shape.

2. THEORETICAL MODEL

In the CZ crystal growth of an oxide, radio-frequency (RF) induction heating is frequently used, as shown in Fig. 1. The a.c. electric current in the coil induces the eddy current in the metal crucible wall. The raw material of the crystal in the crucible is melted by joulean heating from the eddy current. Therefore, in the global analysis of heat transfer in the inductively heated CZ furnace, the electro-magnetic field in the system should be computed first of all to obtain the heat power distributions in the crucible, and then flow and temperature fields in the furnace are calculated.

The numerical algorithm developed in our previous work [11] for calculating the electro-magnetic flow and temperature fields as well as all interface shapes in the inductively heated CZ furnace, is extended to incorporate the efficient method for accounting for the internal radiation within the crystal and the melt. In the interest of brevity, details of the mathematics to calculate the electro-magnetic field in the furnace, the melt hydrodynamics and all interface shapes are not included here, and are available in our previous work [11]. Only a few important points for internal radiative heat transfer are presented here, in which radiative heat transfer in the semitransparent crystal and melt is approximated using a differential (P_1) approximation [18].

The dimensionless forms of the governing equations of the energy and radiative transfer in the melt and the crystal are expressed as follows:

$$Pr\left(u_l\frac{\partial T_l}{\partial r}+w_l\frac{\partial T_l}{\partial z}\right)=\frac{1}{r}\frac{\partial}{\partial r}\left(r\kappa_l\frac{\partial T_l}{\partial r}\right)+\frac{\partial}{\partial z}\left(\kappa_l\frac{\partial T_l}{\partial z}\right)+a_l N_R(J_l-n_l^2T_l^4) \quad (1)$$

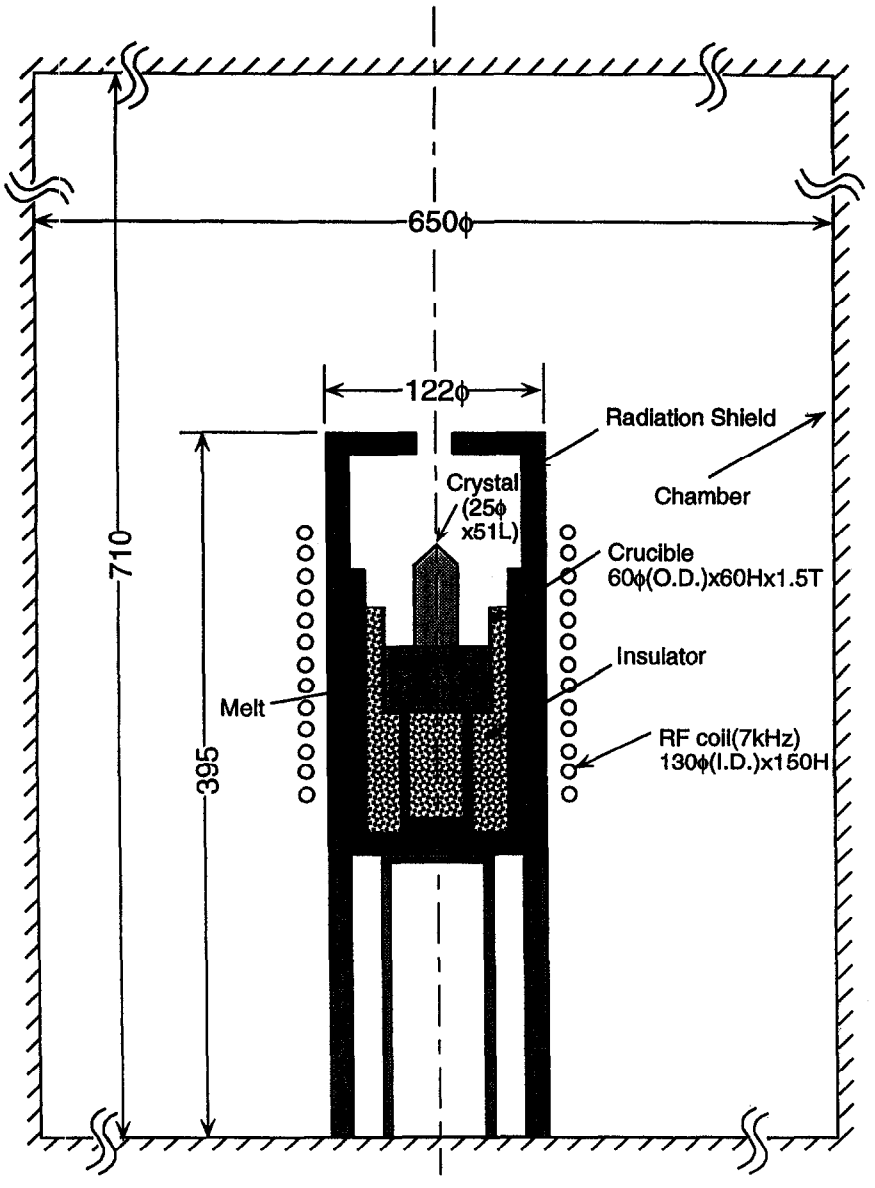

Fig. 1. Schematic diagram of inductively heated CZ furnace.

$$Pe\frac{\partial T_s}{\partial z}=\frac{1}{r}\frac{\partial}{\partial r}\left(r\kappa_s\frac{\partial T_s}{\partial r}\right)+\frac{\partial}{\partial z}\left(\kappa_s\frac{\partial T_s}{\partial z}\right)+a_s N_R(J_s-n_s^2T_s^4) \quad (2)$$

$$\frac{1}{3a_l}\left\{\frac{1}{r}\frac{\partial}{\partial r}\left(r\frac{\partial J_l}{\partial r}\right)+\frac{\partial}{\partial z}\left(\frac{\partial J_l}{\partial z}\right)\right\}=a_l(J_l-n_l^2T_l^4) \quad (3)$$

$$\frac{1}{3a_s}\left\{\frac{1}{r}\frac{\partial}{\partial r}\left(r\frac{\partial J_s}{\partial r}\right)+\frac{\partial}{\partial z}\left(\frac{\partial J_s}{\partial z}\right)\right\}=a_s(J_s-n_s^2T_s^4) \quad (4)$$

where subscripts l and s represent the melt and the crystal, respectively. In the energy equations (1) and (2), the last terms on the right-hand side describe the contribution of radiative heat transfer. a and N_R are the optical thickness and radiation–conduction interaction parameter defined by $a'r_c'$ and $4\sigma T_m'^3 r_c'/k_l$, respectively, in which the optical absorption coefficient a' is independent of the wavelength, since we consider the radiative transfer in the gray-emitting media. n_l and n_s are the refractive indices of the crystal and the melt. J' $(=4\sigma T_m'^4 J)$ is the integrated mean intensity defined by the zeroth-order moment of radiative intensity i'

$$J'=\int_{\omega=4\pi} i'\,d\omega. \quad (5)$$

The boundary conditions for equations (1)–(4) are given by the following equations.

For the energy equations

At the melt–crystal interface

$$-\kappa_l \nabla T_l \cdot \mathbf{n} + \kappa_s \nabla T_s \cdot \mathbf{n} - \frac{N_R}{3a_l} \nabla J_l \cdot \mathbf{n} + \frac{N_R}{3a_s} \nabla J_s \cdot \mathbf{n} = -Pe\, St(\mathbf{e}_z \cdot \mathbf{n}) \quad (6)$$

at the melt free surface

$$-\kappa_l \nabla T_l \cdot \mathbf{n} = \frac{\varepsilon_l N_R}{4} \left\{ \left(1 + n_l^2 + \frac{\varepsilon_l}{1+\rho_l} n_l^2\right) T_l^4 - \frac{2}{1+\rho_l} J_l - \left(1 - \frac{n_l^2}{1+\rho_l} \tau_l\right) q_{i,l}^{out} \right. \quad (7)$$

at the crucible wall

$$-\kappa_l \nabla T_l \cdot \mathbf{n} + \kappa_c \nabla T_c \cdot \mathbf{n} = \frac{\varepsilon_c N_R}{2(2-\varepsilon_c)} (n_l^2 T_l^4 - J_l) \quad (8)$$

at the crystal surface

$$-\kappa_s \nabla T_s \cdot \mathbf{n} = \frac{\varepsilon_s N_R}{4} \left\{ \left(1 + n_s^2 + \frac{\varepsilon_s}{1+\rho_s} n_s^2\right) T_s^4 - \frac{2}{1+\rho_s} J_s - \left(1 - \frac{n_s^2}{1+\rho_s} \tau_s\right) q_{i,s}^{out} \right\} \quad (9)$$

elsewhere

$$-\kappa_k \nabla T_k \cdot \mathbf{n} = \frac{\varepsilon_k N_R}{4} (T_k^4 - q_{i,k}^{out}). \quad (10)$$

For the equation of radiative transfer

At the melt–crystal interface

$$J_l = J_s \quad -\frac{1}{3a_l} \nabla J_l \cdot \mathbf{n} = -\frac{1}{3a_s} \nabla J_s \cdot \mathbf{n} \quad (11)$$

at the melt free surface

$$-\frac{1}{3a_l} \nabla J_l \cdot \mathbf{n} = \frac{1}{2} \left(\frac{1-\rho_l}{1+\rho_l}\right) \left\{ J_l - \frac{n_l^2}{1-\rho_l} (\varepsilon_l T_l^4 + \tau_l q_{i,l}^{out}) \right\} \quad (12)$$

at the crucible wall

$$-\frac{1}{3a_l} \nabla J_l \cdot \mathbf{n} = \frac{\varepsilon_c}{2(2-\varepsilon_c)} (J_l - n_l^2 T_l^4) \quad (13)$$

at the crystal surface

$$-\frac{1}{3a_s} \nabla J_s \cdot \mathbf{n} = \frac{1}{2} \left(\frac{1-\rho_s}{1+\rho_s}\right) \times \left\{ J_s - \frac{n_s^2}{1-\rho_s} (\varepsilon_s T_s^4 + \tau_s q_{i,s}^{out}) \right\} \quad (14)$$

at the center line

$$\nabla J_k \cdot \mathbf{n} = 0. \quad (15)$$

To derive the above boundary conditions, it is assumed that the crystal and the melt are bounded by vanishingly thin semitransparent diffuse-gray surfaces with an emissivity ε, reflectivity ρ and transmissivity τ, and that the crucible wall is an opaque diffuse-gray surface. The interreflections between the crystal or melt surfaces and the surroundings, such as the exposed crucible wall, insulator and radiation shield are accounted for by the incoming radiative flux from the surroundings to the surfaces q_i^{out}, which is obtained in the following manner [19].

An enclosure having N semitransparent diffuse-gray surfaces with uniform temperature is considered, where the enclosure may correspond to the gas space surrounded by the crystal surface, the melt surface, the exposed crucible wall, the insulator, etc. For a typical surface, A_k, let G_{jk} be the fraction of the outgoing radiative flux from surface A_j that reaches A_k. The total outgoing flux from surface A_j is $A_j(\varepsilon_j T_j^4 + \tau_j q_{i,j}^{in}/n^2)$, in which the first term is the emission from the surface A_j and the second is the transmission of the radiative fluxes to surface A_j from the outside of the enclosure, in other words from the inside of the crystal or the melt. The portion traveling by a direct path to A_k is expressed by $A_j(\varepsilon_j T_j^4 + \tau_j q_{i,j}^{in}/n^2) F_{jk}$ with the view factor F_{jk}. The portion which starts from A_j and arrives at A_n is reflected as $A_j(\varepsilon_j T_j^4 + \tau_j q_{i,j}^{in}/n^2) F_{jn} \rho_n$. According to the definition of G_{jk}, all the energy which arrives at A_k originating from A_j is

$$\begin{aligned} &A_j(\varepsilon_j T_j^4 + \tau_j q_{i,j}^{in}/n^2) G_{jk} \\ &= A_j(\varepsilon_j T_j^4 + \tau_j q_{i,j}^{in}/n^2) F_{jk} + \{A_j(\varepsilon_j T_j^4 + \tau_j q_{i,j}^{in}/n^2) F_{j1} \rho_1 G_{1k} \\ &\quad + \cdots + A_j(\varepsilon_j T_j^4 + \tau_j q_{i,j}^{in}/n^2) F_{jk} \rho_k G_{kk} \\ &\quad + \cdots + A_j(\varepsilon_j T_j^4 + \tau_j q_{i,j}^{n}/n^2) F_{jN} \rho_N G_{Nk}. \end{aligned} \quad (16)$$

Dividing equation (16) by $A_j(\varepsilon_j T_j^4 + \tau_j q_{i,j}^{in}/n^2)$, the fraction G_{jk} is given as follows:

$$G_{jk} = F_{jk} + F_{j1} \rho_1 G_{1k} + \cdots + F_{jk} \rho_k G_{kk} + \cdots + F_{jN} \rho_N G_{Nk}. \quad (17)$$

For each surface A_k in the N-sided enclosure, we calculate $G_{1k}, G_{2k}, \ldots, G_{Nk}$ by solving the following set of equations, which is obtained by letting j in equation (17) take all values from 1 to N.

$$\begin{bmatrix} F_{11}\rho_1 - 1 & F_{12}\rho_2 & \cdots & \cdots \\ F_{21}\rho_1 & F_{22}\rho_2 - 1 & \cdots & \cdots \\ \cdots & \cdots & \cdots & \cdots \\ F_{N1}\rho_1 & F_{N2}\rho_2 & \cdots & F_{NN}\rho_N - 1 \end{bmatrix} \begin{bmatrix} G_{1k} \\ G_{2k} \\ \cdot \\ G_{Nk} \end{bmatrix} = - \begin{bmatrix} F_{1k} \\ F_{2k} \\ \cdot \\ F_{Nk} \end{bmatrix}. \quad (18)$$

With G_{jk}, $q_{i,k}^{out}$ in the boundary conditions is obtained using the following equation:

$$q_{i,k}^{out} = \sum_{j=1}^{N} A_j(\varepsilon_j T_j^4 + \tau_j q_{i,j}^{in}/n^2) G_{jk} \quad (19)$$

where

Table 1. Optical properties of the melt and the crystal

Refractive index	
melt (n_l)	2.3
crystal (n_s)	2.3
Absorption coefficient	
melt (a_l') [m^{-1}]	35.1–350.1
crystal (a_s') [m^{-1}]	35.1–280.7
Emissivity	
melt (ε_l)	0.3
crystal (ε_s)	0.3
Reflectivity	
melt (ρ_l)	0.3, 0.7
crystal (ρ_s)	0.3, 0.7
Transmissivity	
melt (τ_l)	0.4, 0.0
crystal (τ_s)	0.4, 0.0

$$q_{i,j}^{\text{in}} = \frac{J_j}{4} - \frac{1}{6a}\nabla J_j \cdot \mathbf{n}. \tag{20}$$

To solve the above problem, the Galerkin finite element method is used. The calculation domain is discretized by isoparametric quadrilateral elements, where the total number of elements and nodal points are 4240 and 4374 in the analysis of the electromagnetic field, and 1095 and 4664 in the flow and temperature fields, respectively. In each element, magnetic stream functions are approximated with a bilinear trial function, velocity vectors, radiative intensity and temperature with biquadratic functions, and pressure with a linear function [11].

3. RESULTS AND DISCUSSION

In the present work, we consider the same geometry of a CZ furnace as that in the previous work [11], where a $LiNbO_3$ single crystal (25 mm diameter) is pulled continuously at the rate of 1 mm h^{-1} from the melt in the Pt crucible (60 $mm^{O.D.} \times 60$ $mm^{H} \times 1.5$ mm^{T}), as shown in Fig. 1. The physical properties and processing parameters used in the calculations are identical to those in our previous work [11] except for the optical properties, e.g. the optical absorption coefficient, refractive index and surface radiative properties. The optical properties of the melt and the crystal are assumed as listed in Table 1, because they are not known at temperatures corresponding to the growth conditions. The Prandtl number, Pr, and the Grashof number, Gr, in this system are 13.6 and 4.67×10^5, respectively, but both the Marangoni number and the crystal rotational Reynolds number are zero, i.e. Marangoni flow is not considered and the crystal is not rotated.

Figure 2 shows the effect of optical thickness, $a(=a'r_c')$, on the temperature distributions in the furnace and the flow pattern in the melt, where the optical absorption coefficients of the crystal and the melt are the same. The boundary surfaces of the melt and crystal are assumed to be semitransparent ones with $\varepsilon_l = \varepsilon_s = 0.3$, $\rho_l = \rho_s = 0.3$ and $\tau_l = \tau_s = 0.4$. When the melt and the crystal are semitransparent, as shown in Fig. 2b and c, the structure of the flow field in the melt is much different from that in the opaque melt ($a = \infty$ in Fig. 2a). In the opaque melt, a vortex center locates relatively higher and nearer the crucible wall, and also the flow exhibits an undulating structure at the bottom of the crucible due to a retarding force caused by vertical stratification of the melt [15]. While, in the semitransparent melt, such an undulating structure does not appear, the relatively simple convection with the vortex center at the middle part of the melt exists, although the intensity of convection in the semitransparent melt is much larger than that in the opaque one. This is due to the larger heat loss through the melt surface by the internal radiation, which

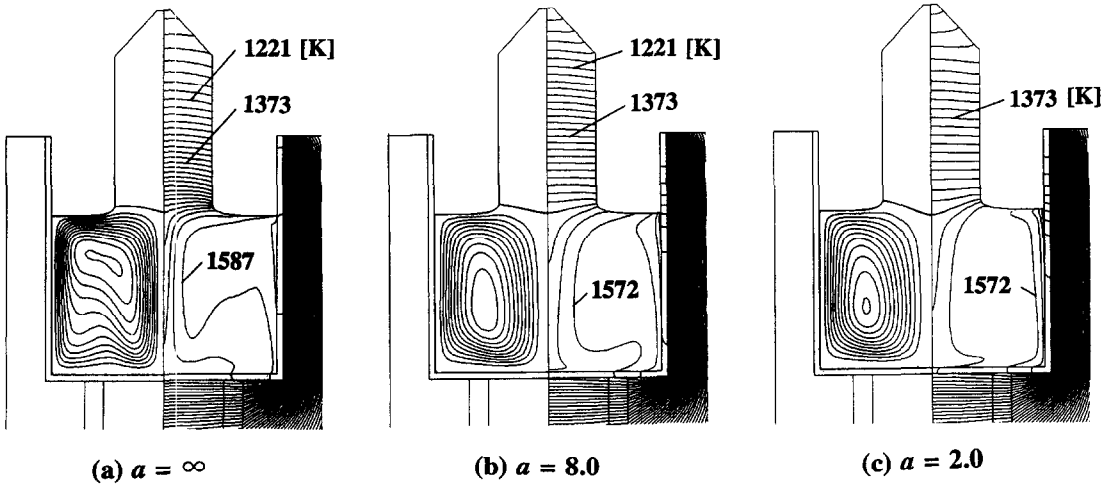

(a) $a = \infty$ (b) $a = 8.0$ (c) $a = 2.0$

Fig. 2. Streamlines in the melt (left side) and isotherms in the furnace (right side) for different values of the optical thickness a, where $a = a_s = a_l$, $\varepsilon_s = \varepsilon_l = 0.3$, $\rho_s = \rho_l = 0.3$, $\tau_s = \tau_l = 0.4$. The contour intervals for the stream functions are (a) 0.1 and (b), (c) 0.4, and for temperature is 15.26 [K]. The maximum values of stream function and temperature in the furnace are (a) 1.11 and 1608 [K], (b) 4.32 and 1716 [K], and (c) 4.43 and 1729 [K], respectively.

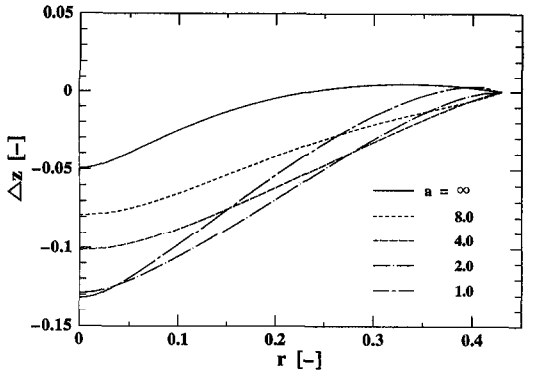

Fig. 3. Effect of the optical thickness a on the melt–crystal interface shape, where $a = a_s = a_l$, $\varepsilon_s = \varepsilon_l = 0.3$, $\rho_s = \rho_l = 0.3$, $\tau_s = \tau_l = 0.4$.

results in an increase in the heat power to keep the crystal radius constant, i.e. the increase in the maximum temperature at the crucible wall. Consequently, a larger temperature gradient is horizontally established across the melt and thus the buoyant flow in the semitransparent melt is stronger than the corresponding flow in the opaque melt. The temperature gradients in the crystal decrease as the optical thickness decreases, because the contribution of the internal radiation into the total heat transfer through the crystal increases and the role of the thermal conduction diminishes.

Figure 3 shows the effect of the optical thickness on the melt–crystal interface shapes when $\varepsilon_l = \varepsilon_s = 0.3$ and $\rho_l = \rho_s = 0.3$. In this figure, Δz represents the deflection of the interface against the flat one, and the negative value of Δz corresponds to a convex interface toward the melt. As the optical thickness decreases, the melt–crystal interface becomes more convex to the melt. Since the internal radiation in a semitransparent crystal enhances the heat flux through the crystal, a larger melt–crystal interface area is needed and the deflection of the interface toward the melt is increased to compensate for the larger heat flux. Cockayne *et al.* [12] experimentally showed that the melt–crystal interface becomes more convex as the molecular porportion of YAG increases during the CZ growth of the mixed garnet crystal formed between YAG and DyAG, where the optical absorption coefficient of YAG is relatively smaller than that of DyAG. The results in Fig. 3 qualitatively explain Cockayne's experimental results.

In Figs. 2 and 3, the oxide melt is assumed to be semitransparent as well as the crystal. However, Nason *et al.* [20] revealed using spectroscopic measurements of the oxide that the optical absorption coefficient of the oxide melt is significantly larger than that of the crystal, although, strictly speaking, their results are valid only at a wavelength of 543 nm because they used a He–Ne laser as a light source. Thus, the absorption coefficient of the $LiNbO_3$ melt may be larger than that of the crystal. Figure 4 shows the calculated results of the temperature distributions in the furnace and the flow pattern in the melt, where a_s is fixed at 2.0 but a_l is varied. In Fig. 4, the melt surface is assumed to be opaque, i.e. $\varepsilon_l = 0.3$ and $\rho_l = 0.7$. The temperature gradients in the melt, especially near the melt–crystal interface, increases with a_l, because the increase in the absorption coefficient of the melt diminishes the role of the radiative heat transfer through the melt and thus increases the role of thermal conduction. The effect of a_l on the shapes of the melt–crystal interface is shown in Fig. 5.The interface becomes more convex to the melt as a_l increases. The radiative heat flux from the melt to the melt–crystal interface decreases as a_l increases, but the total heat flux through the crystal is almost the

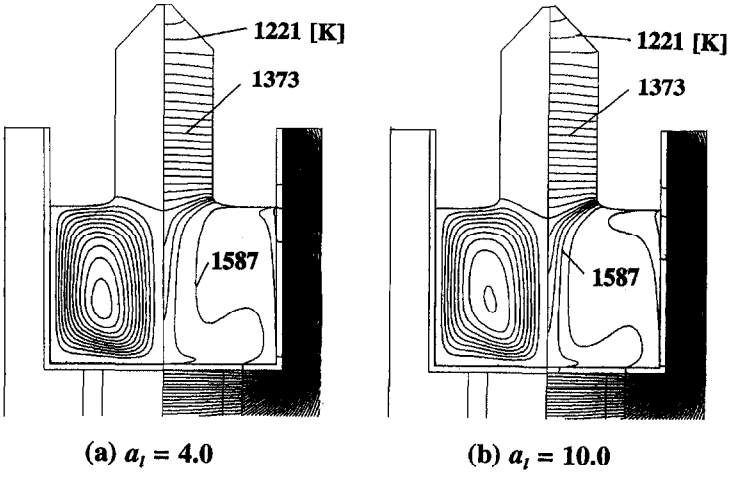

Fig. 4. Streamlines in the melt (left side) and isotherms in the furnace (right side) for different values of the optical thickness of the melt a_l, where a_s is fixed (2.0), and $\varepsilon_s = \varepsilon_l = 0.3$, $\rho_s = 0.3$, $\rho_l = 0.7$, $\tau_s = 0.4$ and $\tau_l = 0$. The contour interval for the stream functions is 0.3 and for temperature is 15.26 [K]. The maximum values of stream function and temperature in the furnace are (a) 3.45 and 1658 [K], and (b) 2.72 and 1671 [K], respectively.

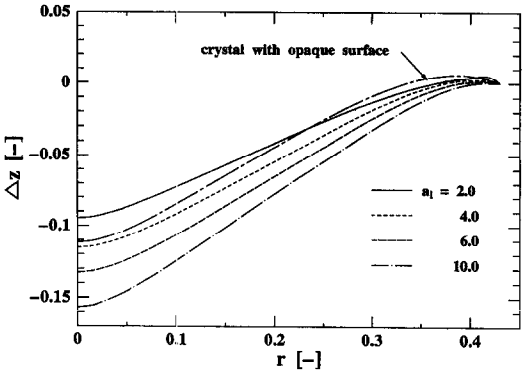

Fig. 5. Effects of the optical thickness of the melt a_l, on the melt–crystal interface shape, where $a_s = 2.0$, $\varepsilon_s = \varepsilon_l = 0.3$, $\rho_s = 0.3$, $\rho_l = 0.7$. This figure also includes the result with opaque crystal surface ($\rho_s = 0.7$).

same, regardless of a_l. This causes large temperature gradients in the melt and deep interface deflection toward the melt to increase.

During the crystal growth of the oxide, crystal surfaces are often coated by impurities deposited by the vapor-phase transport, such as metallic species from the crucible. In such a case, the assumption of an opaque crystal surface may be reasonable [14]. Figure 6 shows the calculated results of the temperature distributions in the furnace and the flow pattern in the melt under the conditions of zero transmissivity of melt and crystal surfaces, i.e. $\varepsilon_l = \varepsilon_s = 0.3$, $\rho_l = \rho_s = 0.7$ and $\tau_l = \tau_s = 0$. Here, the optical thicknesses, i.e. the absorption coefficients, of the crystal and the melt are the same as those in Fig. 4b. The temperature gradient in the crystal is much smaller than those with the semitransparent surfaces shown in Fig. 4b. For the opaque surface and higher value of crystal surface reflectivity, an amount of radiative

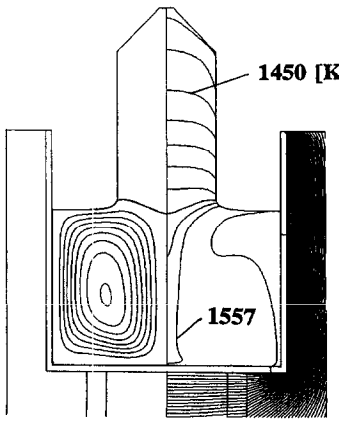

Fig. 6. Streamlines in the melt (left side) and isotherms in the furnace (right side) under the condition that the crystal surface is opaque, where $a_s = 2.0$, $a_l = 10.0$, $\varepsilon_s = \varepsilon_l = 0.3$, $\rho_s = \rho_l = 0.7$. The contour interval for the stream functions is 0.3 and for temperature is 15.26 [K]. The maximum values of stream function and temperature in the furnace are 2.43 and 1592 [K].

flux to the crystal surface is reflected back into the crystal. Thus, the conductive flux normal to the surface and the average temperature in the crystal increase, and the melt–crystal interface becomes less convex to the melt, as shown in Fig. 5.

4. CONCLUSIONS

For the crystal growth of an oxide, the global analysis of heat transfer in the inductively heated CZ furnace was developed, which took the radiative heat transfer within the crystal and the melt into account. The effect of the optical properties of the melt and the crystal, i.e. the optical absorption coefficient, and surface emissivity, reflectivity and transmissivity, on the flow and temperature fields in the CZ furnace and on the melt–crystal interface shape was theoretically investigated. It is found that the flow and temperature fields are strongly affected by the internal radiation in the crystal and the melt, and that the melt–crystal interface shape becomes more convex to the melt as the optical absorption coefficients of both the crystal and the melt decrease. However, the deflection of the interface becomes larger as the absorption coefficient of the melt increases when the absorption coefficient of the crystal is fixed.

Acknowledgements—This work was supported in part by a Grant-in-Aid for Scientific Research (no. 05239106) from the Ministry of Education, Science and Culture, Japan.

REFERENCES

1. N. Kobayashi, Hydrodynamics in Czochralski growth—computer analysis and experiments, *J. Crystal Growth* **52,** 425–434 (1981).
2. N. Kobayashi, Difficulties encountered in Czochralski growth of some oxide single crystals, *J. Crystal Growth* **55,** 339–344 (1981).
3. W. E. Langlois, Effect of the buoyancy parameter on Czochralski bulk flow in garnet growth, *J. Crystal Growth* **46,** 743–746 (1979).
4. J. J. Derby and Q. Xiao, Some effects of crystal rotation on large-scale Czochralski oxide growth, *J. Crystal Growth* **113,** 575–586 (1991).
5. H. Kopetsch, Numerical simulation of the interface inversion in Czochralski growth of oxide crystals, *J. Crystal Growth* **102,** 505–528 (1990).
6. Y. Okano, T. Fukuda, A. Hirata, N. Takano, T. Tsukada, M. Hozawa and N. Imaishi, Numerical study on Czochralski growth of oxide single crystals, *J. Crystal Growth* **109,** 94–98 (1991).
7. P. A. Sackinger, R. A. Brown and J. J. Derby, A finite element method for analysis of fluid flow, heat transfer and free interfaces in Czochralski crystal growth, *Int. J. Numer. Meth. Fluids* **9,** 453–492 (1989).
8. T. Tsukada, N. Imaishi and M. Hozawa, Theoretical study of the flow and temperature fields in CZ single crystal growth, *J. Chem. Engng Jap.* **21,** 184–191 (1988).
9. T. Tsukada, M. Hozawa and N. Imaishi, Effect of interface inversion on thermal stress field in CZ crystal growth of oxide, *J. Chem. Engng Jap.* **23,** 286–290 (1990).
10. J. J. Derby, L. J. Atherton and P. M. Gresho, An integrated process model for the growth of oxide crystals by the Czochralski method, *J. Crystal Growth* **97,** 792–826 (1989).
11. T. Tsukada, M. Hozawa and N. Imaishi, Global analysis

of heat transfer in CZ crystal growth of oxide, *J. Chem. Engng Jap.* **27,** 25–31 (1994).
12. B. Cockayne, M. Chesswas and D. B. Gasson, Facetting and optical perfection in Czochralski growth garnets and ruby, *J. Mater. Sci.* **4,** 450–456 (1969).
13. Ji. Kvapil, Jo. Kvapil, B. Manek, B. Perner, R. Autrata and P. Schauer, Czochralski growth of YAG:Ce in a reducing protective atmosphere, *J. Crystal Growth* **52,** 542–545 (1981).
14. Q. Xiao and J. J. Derby, The role of internal radiation and melt convection in Czochralski oxide growth: deep interfaces, interface inversion, and spiraling, *J. Crystal Growth* **128,** 188–194 (1994).
15. Q. Xiao and J. J. Derby, Heat transfer and interface inversion during the Czochralski growth of yttrium aluminium garnet and gadolinium gallium garnet, *J. Crystal Growth* **139,** 147–157 (1994).
16. S. Brandon and J. J. Derby, Internal radiation transport in the vertical Bridgman growth of semitransparent crystals, *J. Crystal Growth* **110,** 481–500 (1991).
17. S. Brandon and J. J. Derby, Heat transfer in vertical Bridgman growth of oxides: effects of conduction, convection, and internal radiation, *J. Crystal Growth* **121,** 473–494 (1991).
18. H. Matsushima and R. Viskanta, Effects of internal radiation transfer on natural convection and heat transfer in a vertical crystal growth configuration, *Int. J. Heat Mass Transfer* **33,** 1957–1968 (1990).
19. R. Siegel and J. R. Howell, *Thermal Radiation Heat Transfer* (2nd Edn). McGraw-Hill, New York (1981).
20. D. O. Nason, C. T. Yen and W. A. Tiller, Measurements of optical properties of some molten oxides, *J. Crystal Growth* **106,** 221–226 (1990).